nature food

Article

https://doi.org/10.1038/s43016-026-01298-0

Temperature thresholds of extreme heat-induced yield loss in maize and soybean reveal geographic heterogeneity across the Northern Hemisphere

Received: 7 October 2024

Accepted: 9 January 2026

Published online: 18 February 2026

Check for updates

Quanbo Zhao[1,16], Chenzhi Wang[1,2,16], Xuhui Wang[1] ✉, Ehsan Eyshi Rezaei[2], Christoph Müller[3], Enli Wang[4], Heidi Webber[2,5], Liangliang Zhang[1], Xiangyi Li[1], Yuxing Sang[1], Gang Zhao[6,7], Christian Folberth[8], Atul Jain[9], Wenfeng Liu[10], Masashi Okada[11], Florian Zabel[12], Jonas Jäegermeyr[13,14], Hui Guo[1], Yao Zhang[1], Yu Jiang[15], Feng Zhou[1] & Shilong Piao[1]

Exposure to extreme high temperatures is a major constraint on global crop productivity, yet most large-scale assessments rely on fixed temperature thresholds that overlook regional variation in genetics, environment and management. Consequently, the temperature thresholds at which heat exposure begins to cause substantial yield loss and their spatial variability remain unclear. Here we compiled subnational yield census over Northern Hemisphere (20° N–55° N) and analysed the extreme degree days (EDDs) to estimate a data-driven critical threshold ($EDD_{threshold}$). Our findings reveal $EDD_{threshold}$ for maize and soybean are 34.8 ± 4.0 °C and 33.7 ± 3.9 °C, respectively. In contrast, state-of-the-art crop models significantly underestimated $EDD_{threshold}$ and its spatial variations, leading to overestimated extreme heat exposure, partially explaining their underestimate in yield loss during extreme heat events. We estimate that without adaptations, growing-season extreme heat exposure could increase by 2.4%–16.1% for maize and 4.9%–16.0% for soybean by the end of the century, and sowing-date adjustment alone cannot fully offset the projected increase in extreme heat exposure.

Extreme heat is a widely recognized threat to global food security[1]. It accelerates premature crop senescence, damages photosynthetic organs and causes yield losses[2–6]. Recent estimates suggested that extreme heat events account for around 10% of annual global cereal production losses globally[7], equivalent to over 1 month's requirements for the global population. The increasing frequency of extreme heat events in breadbasket regions further destabilize global food production[8,9], increasing the risk of food price spikes[10] and exacerbating hunger[11]. When assessing the extreme heat impacts, crop-specific temperature thresholds that define the onset of harmful extreme heat exposure have been widely used at large scale[3,6,12,13], implicitly assuming the thresholds are spatially constant within a given crop. The extreme heat exposure actually experienced by crops, however, could vary spatially as heat impacts are not only shaped by genotypes[14,15] but also by environmental conditions[16–18] and agronomic management (for example irrigation[19–21], which could raise the threshold by ~5 °C (ref. 22)). These drivers differ from region to region, implying pronounced geographic heterogeneity in exposure. Under rapid global warming, the occurrence of high

A full list of affiliations appears at the end of the paper. ✉e-mail: xuhui.wang@pku.edu.cn

temperature is projected to increase[23], which will expose crops to more heat events and further negatively affect food productivity[8,9,24]. The absence of spatially resolved extreme heat threshold constitutes a fundamental limitation in climate vulnerability assessments, hindering better prediction of yield losses under future warming.

Numerous studies have provided evidence that extreme degree days (EDDs)[3,6,25] serve as an effective metric for quantifying the impact of heat stress on crop yields. EDDs are calculated by summing air temperatures that exceed a specific temperature threshold, thus capturing the severity of extreme heat exposure. Consequently, the choice of this threshold ($EDD_{threshold}$) is critical for assessing extreme heat-related risks during the growing season. Above the $EDD_{threshold}$, the exposure to high temperatures results in yield decline substantially[2]. However, most current studies just applied a fixed temperature value across large regions, overlooking spatial variations on the $EDD_{threshold}$. Whereas some studies set the threshold for maize and soybean around 40 °C (refs. 12,13,26), in others, heat stress may already arise below 30 °C (refs. 9,27,28), leading to inconsistencies in estimating extreme heat exposure.

Here we harmonized yield records over nearly 8,000 districts or counties to provide an estimation on the $EDD_{threshold}$ for maize and soybean at fine spatial scale across major breadbasket regions of the Northern Hemisphere. Our study regions generally supply two-thirds of global maize production and half of global soybean production (Fig. 1a,b). With our new estimated $EDD_{threshold}$, we then projected future change in extreme heat exposure for maize and soybean based on outputs from 11 global gridded crop models (GGCMs). We also evaluated the potential difference of the projected extreme heat exposure that arises from using widely applied spatially fixed threshold (30 °C (refs. 2,3,29,30)) with our $EDD_{threshold}$. Finally, we assessed how growing-season adaptations by advanced sowing dates and adoption of long-maturity cultivars may help crops to escape extreme heat exposure.

Estimation of the $EDD_{threshold}$ in the Northern Hemisphere

Using detailed county-level yield datasets from major producing regions in the Northern Hemisphere, we derived the spatial pattern of $EDD_{threshold}$ for maize and soybean (Fig. 1c–f). The average (± standard deviation) $EDD_{threshold}$ for maize was 34.8 ± 4.0 °C (median: 35.0 °C; interquartile range (IQR) equals: 31.2 °C to 38.4 °C), while for soybean was 33.7 ± 3.9 °C (median: 35.0°C; interquartile range (IQR) equals: 31.4 °C to 38.8 °C), respectively (Fig. 1c–f). Both crops showed strong spatial heterogeneity. Higher $EDD_{threshold}$ for maize was found in South Europe, northwestern China and midwestern USA, whereas higher soybean thresholds were detected mainly in the North China Plain and central USA (Fig. 1c,d).

We verified the robustness of $EDD_{threshold}$ for both crops under multiple methodological assumptions, grouped by three types: regression structure modifications, climate data-source alternatives and growth stage definition adjustments (Methods and Supplementary Figs. 1–12). Our results revealed that first, the distribution of $EDD_{threshold}$ remained nearly unchanged when altering the parameters of base temperature (Supplementary Figs. 1 and 2). Second, different model structures on the interpretation of growing degree days (GDDs), yield detrending, proxies of water availability, the consideration of other explanatory variables and different choices on climate datasets resulted in minimal differences, while the $EDD_{threshold}$ estimates in majority regions were significantly correlated and similarly distributed (Supplementary Figs. 3–11). Third, even when isolating the critical stage of anthesis and grain filling (AGF) from the growing season, a period expected to amplify sensitivity, only minor differences on $EDD_{threshold}$ were observed (Supplementary Fig. 12). These tests confirm that our methods are robust in assessing extreme heat exposure that causes yield loss across diverse analytical frameworks.

We further benchmarked our estimates on $EDD_{threshold}$ against prior experimental and observational studies and found broad consistency with reported thresholds in the observation locations (Supplementary Table 1). These spatial variations were difficult to be explained in these sporadic studies, but our analyses on the pan-Northern Hemisphere pattern showed that climatic factors account for ~30% of the observed variance (Supplementary Figs. 13 and 14, and Supplementary Notes). Management factors, such as irrigation, also had a significant impact on $EDD_{threshold}$. In counties where irrigated and rain-fed systems coexisted over midwestern USA, $EDD_{threshold}$ was significantly higher under irrigated management by approximately 1.1 °C for maize ($P = 0.009$) and 3.5 °C for soybean ($P < 0.001$) (Supplementary Fig. 15).

Crop models underestimate the variability of the $EDD_{threshold}$

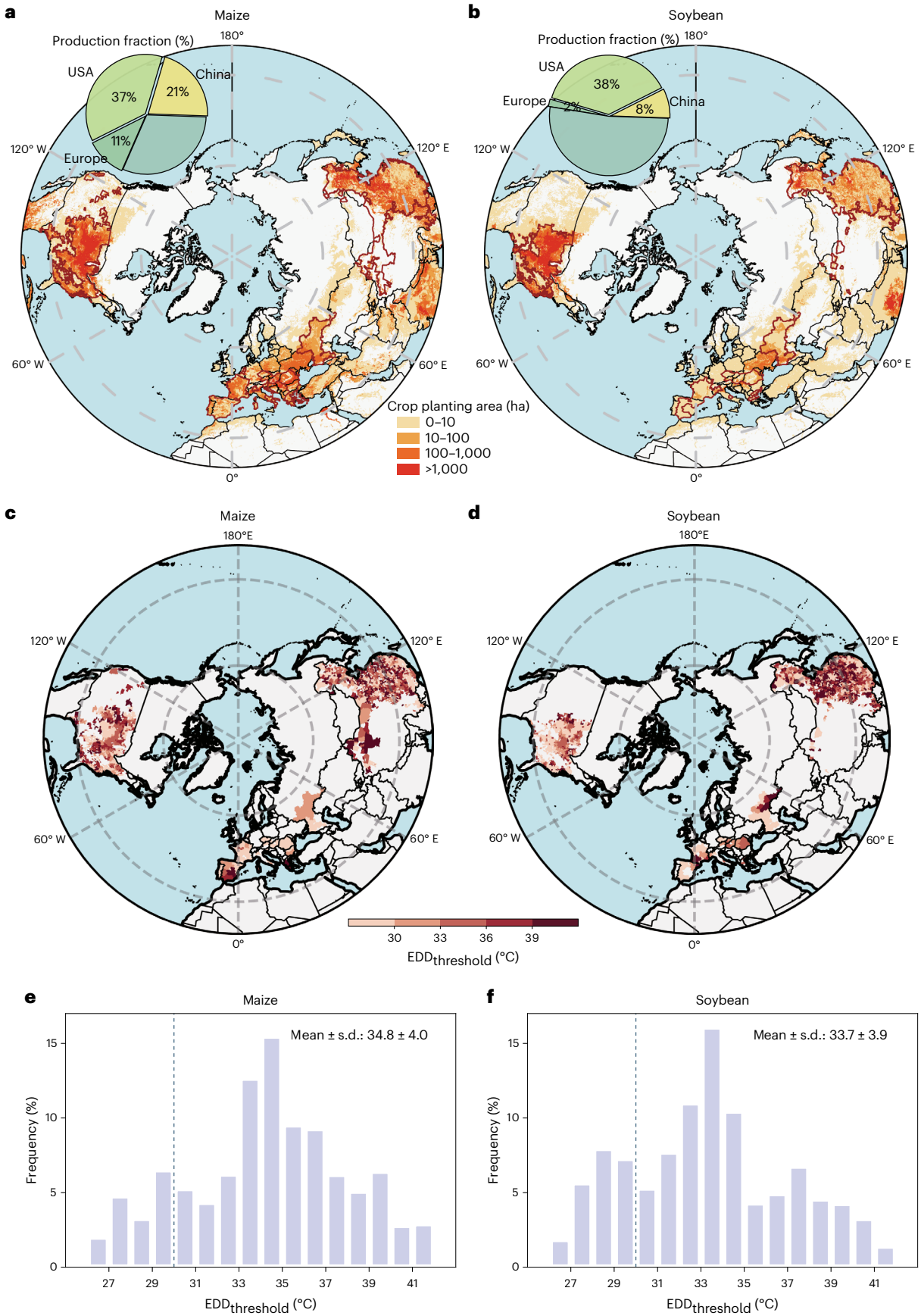
To assess the capacity of global crop models in capturing extreme heat exposure, we applied the same data-driven approach to hindcast spatial variations in $EDD_{threshold}$ using 11 state-of-the-art global crop models. The ensemble of these GGCMs, driven by five different climate models, showed a much narrower range of the spatial variations of $EDD_{threshold}$ than observation (Fig. 2a,b). This systematic bias persisted not only in the model ensemble but also in each individual model (Supplementary Fig. 16). This could be attributed to the lack of representation in spatial variations of cultivar and agronomic parameters across regions, and incomplete parameterization of the physiological responses to extreme temperatures (Supplementary Table 2). In particular, most models underestimated $EDD_{threshold}$ for maize (Fig. 2c) that the ensemble-mean $EDD_{threshold}$ was 1.5 °C lower than observed $EDD_{threshold}$ (ranging from −2.5 °C to 0.3 °C across individual models) for maize and only 0.4 °C lower (ranging from −1.5 °C to 1.7 °C) for soybean (Fig. 2c,d). Further decomposition of the source of the bias revealed that crop models are more responsible than the climate models for underestimating $EDD_{threshold}$ variability (Fig. 2c,d).

Projected increase in future extreme heat exposure

Leveraging our spatially explicit $EDD_{threshold}$, we found a substantial increase in extreme heat exposure for maize and soybean by mid-century (2041–2060) and towards the end of this century (2081–2100) (Fig. 3a–d and Supplementary Fig. 17). During the baseline period (2000–2019), the observed average extreme heat exposure normalized by growing-season duration were 7.8% (9.8 days) and 9.1% (11.3 days) for maize and soybean, respectively. By the end of the century, even under the low-emissions scenario (Shared Socioeconomic Pathway 1-2.6), these values rise to 10.2% (12.0 days) for maize and 11.9% (13.9 days) for soybean (Fig. 3a–d and Supplementary Fig. 17). In contrast, the high-emissions scenario (SSP5-8.5) leads to far more severe impacts,

Fig. 1 | Spatial patterns of $EDD_{threshold}$ in major maize and soybean breadbaskets across the mid- to high-latitudinal Northern Hemisphere. a,**b**, Spatial patterns of planting area for maize (**a**) and soybean (**b**) based on Spatial Production Allocation Model (SPAM) (data from ref. 49). The red lines indicate study regions. Insets show the proportion of total global production within the study area (categorized by the USA, China and Europe). Note that only regions with consecutive yield records and detectable threshold (that is, experienced high-temperature exposure in growing season) are included. **c**,**d**, Spatial patterns of $EDD_{threshold}$ for maize (**c**) and soybean (**d**). **e**,**f**, Histograms of $EDD_{threshold}$ for maize (**e**) and soybean (**f**), weighted by regional plant area. The dashed line represents 30 °C. s.d., standard deviation. Basemap data in **a**–**d** from Natural Earth (https://www.naturalearthdata.com; USA), Eurostat (https://ec.europa.eu/eurostat/web/gisco/geodata/statistical-units/territorial-units-statistics; EU), Simple Maps (https://simplemaps.com/gis/country/ru; Russia) and the Standard Map Service (https://cloudcenter.tianditu.gov.cn/administrativeDivision; China).

https://doi.org/10.1038/s43016-026-01298-0



https://doi.org/10.1038/s43016-026-01298-0

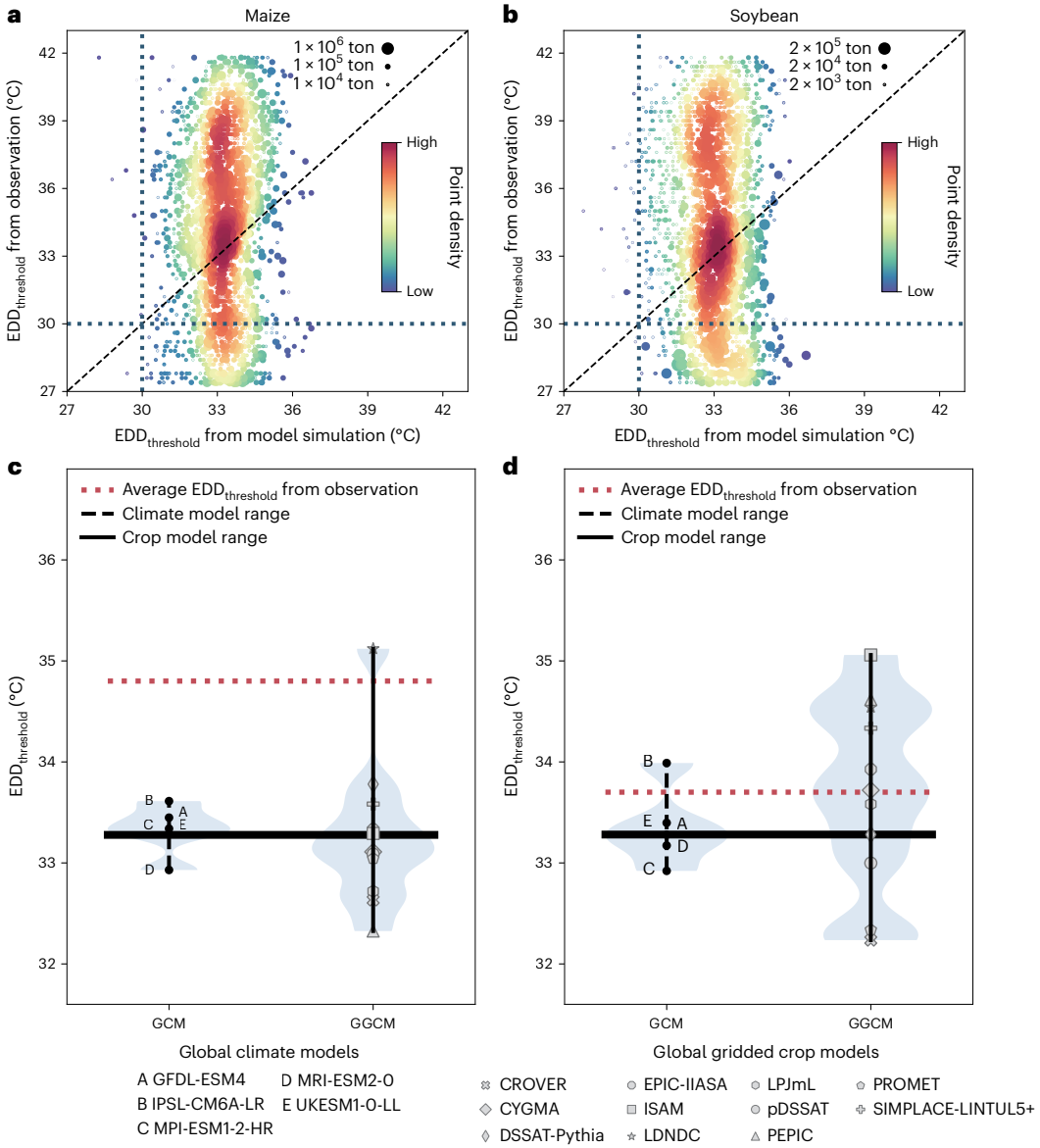


Fig. 2 | Comparison with $EDD_{threshold}$ estimation from process-based crop models. a,**b**, Scatter plots of $EDD_{threshold}$ derived from climate and crop models and $EDD_{threshold}$ derived from observational datasets for maize (**a**) and soybean (**b**). Each point represents a subnational geographical unit, with point size indicating average production and colour indicating point density. The black dashed line represents 1:1 line. **c**,**d**, The black horizontal lines show average model-derived $EDD_{threshold}$ for maize (**c**) and soybean (**d**), weighted by production. The red dotted lines show the average $EDD_{threshold}$ value from observation. Whiskers indicate the range of global climate models (GCM, dashed line, as the mean across crop models) and the range of GGCMs (solid line, as the mean across climate models). Individual model results are represented by letters and symbols along the whisker lines. Shaded areas describe the distributions of models.

with extreme heat exposure reaching 24.1% (26.2 days) for maize and 25.3% (26.0 days) for soybean—a nearly threefold increase compared to 2000–2019 levels (Fig. 3a–d and Supplementary Fig. 17).

Importantly, ignoring spatial variations in $EDD_{threshold}$ by adopting a fixed 30 °C threshold led to systematic overestimation of extreme heat exposure during both hindcast and projection period (Fig. 3e–h and Supplementary Fig. 18). For maize, the fixed threshold overestimated baseline exposure by 3.3% (6.8 days), increasing to 6.2% (12.2 days) under SSP126 and 9.3% (14.9 days) under SSP585 by mid-century. For soybean, the overestimation was 3.4% (8.2 days) for the baseline and projected to be 7.0% (14.8 days, SSP126) and 10.2% (17.9 days, SSP585) by mid-century. This equates to falsely classifying up to 2 weeks of the growing season as heat stressed in key breadbasket regions of Northern Hemisphere, such as the North China Plain and the US Corn Belt (Fig. 3i–l and Supplementary Fig. 18), which is of particular concern as the misclassification often took place during the AGF stage—the phenological stages when crops are sensitive to thermal variability (Fig. 3), which could partially explain the bias of crop models in assessing impacts of extreme heat events[31].

Growing-season adaptations cannot fully compensate the increasing extreme heat exposure

Though our estimates show less extreme heat exposure than what would be identified using a fixed threshold of 30 °C, a warmer future would thus cause greater extreme heat exposure without adaptation. To assess whether agronomic adaptation, such as adjusting planting dates or extending the growing season[32,33], might mitigate increasing extreme heat exposure, we examined three adaptation scenarios: (1) adjusting sowing dates, earlier sowing in warmer climates, (2) maintaining a fixed growing-season length[34] and (3) a combination of earlier planting and constant growing-season length (Methods). While

https://doi.org/10.1038/s43016-026-01298-0

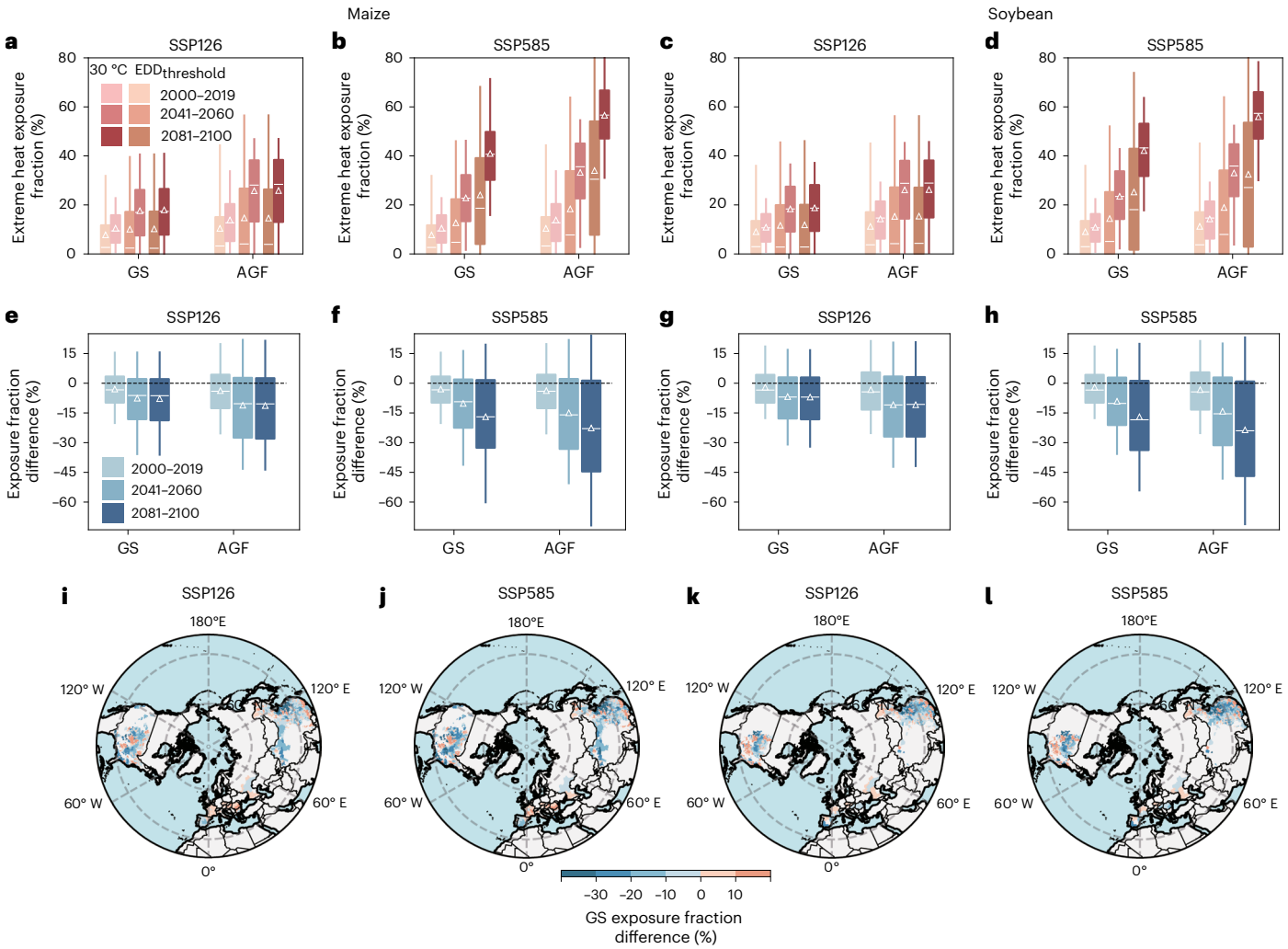


Fig. 3 | Projected fractions of extreme heat exposure and differences between $EDD_{threshold}$ and the prevailing constant threshold for maize and soybean. **a**–**d**, The fraction of extreme heat exposure, expressed as a percentage of the length of the growing season, shown as the multi-year average values across climate and crop models for maize (**a**,**b**) and soybean (**c**,**d**) under SSP126 (**a**,**c**) and SSP585 (**b**,**d**). **e**–**h**, Projected differences (calculated as the difference of extreme heat exposure fraction between by the regional varying $EDD_{threshold}$ and by fixed 30 °C) in growing season for maize (**e**,**f**) and soybean (**g**,**h**) under SSP126 (**e**,**g**) and SSP585 (**f**,**h**). **i**–**l**, Spatial patterns of growing-season exposure fraction differences in 2041–2060 for maize (**i**,**j**) and soybean (**k**,**l**) under SSP126 (**i**,**k**) and SSP585 (**j**,**l**). The box charts (for maize, $n = 3,581$; for soybean, $n = 3,516$) show the distribution of region-specific exposure fraction differences in growing season (GS) and in AGF. Colours ranging from light to dark represent different time periods for historical observation (2000–2019) and future projection (2041–2060 and 2081–2100). The ends of each box and the line inside represent the 25th, median and 75th percentiles, and triangles represent the mean value. Whiskers represent the range of 5th and 95th percentiles. Basemap data in **i**–**l** from Natural Earth (https://www.naturalearthdata.com; USA), Eurostat (https://ec.europa.eu/eurostat/web/gisco/geodata/statistical-units/territorial-units-statistics; EU), Simple Maps (https://simplemaps.com/gis/country/ru; Russia) and the Standard Map Service (https://cloudcenter.tianditu.gov.cn/administrativeDivision; China).

these adaptation scenarios reduced overall extreme heat exposure for both crops compared with the no-adaptation scenario, they failed to fully counteract its escalation. The attenuation effect, however, is scenario dependent: the exposure with adaptation would increase by only 1-2% of the growing season under SSP126 (Fig. 4), while increase by at least 4% under SSP585 in mid-century (Fig. 4) and may double at the end of the century (Supplementary Fig. 19). Moreover, the pronounced surge in extreme heat exposure during anthesis cannot be compensated by the warming-induced acceleration of crop developments[34] (Supplementary Fig. 20). This further highlights the urgency of climate-mitigation actions, without which adaptation efforts would fail in containing the increasing risk of extreme climate events.

Discussion

Accurate depiction of crop exposure to heat stress is fundamental for reliably quantifying extreme heat-induced yield loss and crop failure. Previous studies have adopted spatially invariant but largely different thresholds for assessing extreme heat impact: some considered heat damage to maize and soybean occurs only above approximately 40 °C (refs. 12,13,26), whereas others used thresholds of 30 °C or even lower[9,27]. In addition, spatially fixed thresholds are often applied in many studies and standards. For example, in China, a national standard called 'Temperature index of high temperature harm' (GB/T 21985-2008) also suggest a fixed threshold to be applied over the entire nation, whose climate, over cropping zone vary largely for maize from the south (~20° N) to the north (~50° N). The large discrepancies in defining the threshold result in substantial variations in forecast/hindcast of heat-related risks. In this study, we supplement these experimental thresholds with our estimates from county-level yield statistics, reflecting the onset of yield decline under realized local environments and management. The spatially explicit threshold ($EDD_{threshold}$) for maize and soybean across the Northern Hemisphere demonstrates strong

https://doi.org/10.1038/s43016-026-01298-0

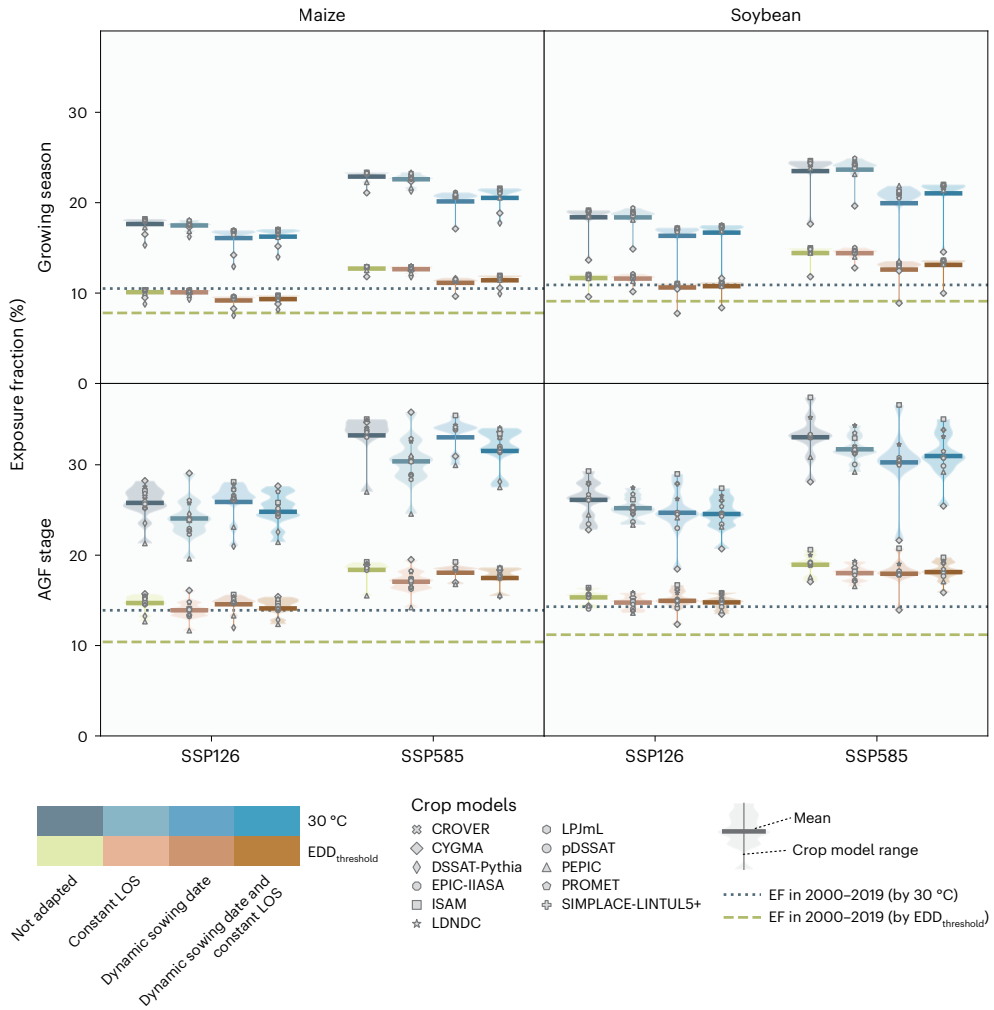


Fig. 4 | The effects of growing-season adaptations on exposure to extreme heat for maize and soybean in 2041–2060, SSP126 and SSP585. Projected future exposure fraction for three adapted growing seasons (Methods), and the default growing season in GGCMI crop models are shown using the spatial varying $EDD_{threshold}$ and the prevailing fixed 30 °C, presented as the average values across models (bold horizontal line). The range of crop models is indicated by the solid vertical lines. Individual model results are denoted by symbols (for maize, $n = 11$; for soybean, $n = 10$), and the model distributions are illustrated by shades. The dashed lines represent the exposure fraction measured by $EDD_{threshold}$ in historical period for corresponding crops and phenological stages. The dotted lines represent the exposure fraction measured by fixed 30 °C in historical period for corresponding crops and phenological stages. LOS, length of growing season.

geographic heterogeneity and help narrowing discrepancies in prior assumptions about extreme heat exposure.

Several drivers of the spatial variations in the $EDD_{threshold}$ could be identified. Our analyses using machine learning models revealed that climatic factors can explain as much as 30% of the spatial variations in $EDD_{threshold}$ (Supplementary Figs. 13 and 14), highlighting climatic adaptation for extreme heat exposure[35]. Soil properties may also play a role, for instance, soils with higher water-holding capacities can buffer compound heat-drought stress, whereas soils with lower water-holding capacities may exacerbate extreme heat impacts[16].

The apparent adaptation, however, may not necessarily be automatic; it could result from breeding efforts[36] or adaptive management such as irrigation. Existing management datasets are spatially coarse and aggregated, which limits detectability of fertilizer and irrigation effects at the global scale, we can only exploited regions where data are available. On the basis of the US county-level irrigation records, we found that $EDD_{threshold}$ is significantly higher under irrigation (Supplementary Fig. 15), consistent with previous studies[22] showing irrigation mitigates exposure to extreme heat. The buffering capacity of irrigation, however, depends on water availability: in water-limited conditions, supplies may be insufficient to prevent deficits in soil moisture; thus irrigation cannot fully alleviate heat stress[37]. Consequently, a significant global signal is not detected even though local effects are clear—an outcome probably driven by the coarse resolution of global irrigation datasets and the inherent spatio-temporal heterogeneity of effective irrigation intensity, rather than any lack of importance of irrigation itself.

A plausible pathway for irrigation to reduce extreme heat exposure is by promoting crop transpiration, which effectively lowers canopy temperature[21,22,38,39], a thermal index found to shape crop heat stress even more than ambient air temperature[39]. However, most current crop models rely only on air temperature to drive heat accumulation, overlooking additional heat stress that dry soil conditions may bring into the micro-environment. Although the importance of canopy temperature for a crop's micro-environment has been widely recognized, using it to force crop models remain challenging: retrieving accurate canopy temperature from satellite remote sensing remains technically difficult[40], rendering global observational datasets of canopy temperature limited. Modelling canopy temperature is also not mature, particularly under concurrent drought and heat stress conditions, failing to reliably capture interactions between canopy temperature and moisture change[41].

In addition, benchmarking our results with state-of-the-art global crop models (Fig. 2 and Supplementary Table 2) further revealed

several important limitations in current simulation of crop responses to extreme heat. For example, crop models are mostly calibrated with experiment or yield census. The prescribed $EDD_{threshold}$ in models typically lower than observed $EDD_{threshold}$ (Fig. 1e,f) causes models to overestimate the extreme heat exposure, but they can still produce similar extreme heat-induced yield loss in the experiments/statistics by lowering modelled crop response to unit heat exposure[42] (vulnerability). Although this compensation between exposure and vulnerability might produce reasonable yield loss in the calibration dataset, when greater extreme heat events come, it would underestimate yield loss (see Schewe et al.[31]) due to its biased vulnerability (Extended Data Fig. 1). Moreover, applying spatially invariant extreme heat exposure thresholds fails to account for regional variation in heat resistance, which could also introduce systematic biases when simulating the impacts of extreme heat events over broader regions.

Looking into the future, the increasing exposure of crops to extreme heat is almost unavoidable. We consistently observed rising trends in extreme heat exposure across most major crop-producing regions in the Northern Hemisphere, regardless of scenarios, climate models and crop models used. Widely discussed adaptation strategies against extreme heat-induced yield loss such as adjusting the sowing dates and adopting new varieties to maintain the growing-season length[32,43,44] are, however, insufficient to fully offset escalating extreme heat exposure, even though considering the sensitive phenological stage to extreme heat could be advanced due to accelerated phenological development (Supplementary Fig. 20). Therefore, addressing the rise in extreme heat exposure requires not only more accurate projections from crop models but also the implementation of diverse and coordinated adaptive management strategies. At the field level, microclimate regulation through precise irrigation scheduling and soil-cover management can further help alleviate excessive heat exposure[21].

The adaptation strategies we discussed above should be integrated into climate-smart agriculture framework[45], implementation of which could be supported by applying our spatially explicit $EDD_{threshold}$. Climate-smart agriculture promotes a holistic approach that not only ensures food security but also enhances the adaptive capacity and resource-use efficiency of agricultural systems, simultaneously achieving climate-mitigation goals through enhanced carbon sequestration and reduced greenhouse gas emissions[45]. As our results show that without effective global action reducing greenhouse gas emissions to limit global warming, the increasing risks of extreme climate events could not be easily adapted. Our choices in greenhouse gas emissions today largely shape the future food-security risks from extreme climate events.

Methods

Yield and ancillary data

The subnational yield data used in this study were obtained from the national statistic agencies during 2000–2019. For the USA, county-level data were obtained from the US Department of Agriculture (USDA) National Agricultural Statistics Service (www.nass.usda.gov). For the European Union and partner countries, NUTS2-level data were obtained from Eurostat (https://ec.europa.eu/eurostat). For Russia, state-level data were obtained from the Federal State Statistics Service (https://rosstat.gov.ru/). For China, county-level data were obtained from the official agricultural statistical year books of each county or province. The yield data were subjected to an outlier filtering according to Schauberger et al.[46] because the statistical annotations were sometimes erroneous with unattainable value. We included only regions with yield records more than 10 years (Supplementary Fig. 23).

To identify regional-level crop development stages including silking or blooming and maturity dates and sowing dates were collected from a combination of site-based observations, statistical progress of crop phenology and satellite-derived data to make a crop calendar (Supplementary Fig. 24). The timing of corresponding stages are fixed as annual high-resolution observations were sparce. For the USA, weekly statistical phenological data were obtained from the USDA National Agricultural Statistics Service (www.nass.usda.gov). For each state-year phenological stage, the week where half of the crops had experienced the stage were chosen to represent for the stage. For China, daily phenological data were obtained from a satellite-derived product ChinaCropPhen[47] for maize at 1 km and from agricultural meteorological stations of the China Meteorological Administration (CMA, data.cma.cn) for soybean. A total of 65 stations with 1,430 site-year records were used in this study. For regions where subnational crop development data are not available, we use GGCMI global crop calendar[48], which is a composite product merging various observational data. The whole growing season was divided into vegetative stage (from sowing or emerging to 10 days before flowering), anthesis (21 days around flowering) and grain filling stage (10 days after flowering to maturity) as described in Lobell et al.[3].

Global distributions of maize and soybean are derived from the Spatial Production Allocation Model (SPAM)[49]. We filtered regions where cropland had more than 5 years heat exposure (daily maximum temperature > 30 °C for more than 1 day within growing season) to assure the regions involved in the analysis did have experienced high temperature (Supplementary Fig. 25). A total of 3,929 counties for maize and 3,779 counties for soybean were selected, with the total number of records at 69,157 for maize and 67,012 for soybean.

Because the statistical yield records in subnational administrative units were not available to separate rain-fed and irrigated systems (only a few counties in the USA provide separated rain-fed and irrigated systems census), we use satellite-based irrigation cropland distribution to calculate the irrigated area fraction (in percentage of plant area). Irrigation distribution for croplands were obtained from Landsat-based Irrigation Dataset (LANID)[50] at 30-m resolution, Eurostat (https://ec.europa.eu/eurostat) and a 500-m resolution irrigated croplands product in China[51]. These data were calibrated by cropland masks to confirm corresponding crops (that is, maize or soybean) were planted, using cropland distributions from the USDA Cropland Data Layer (CDL)[52] for USA or data from SPAM for other regions. Afterwards, the crop-specific irrigation areas were summed at subnational administrative units. We also obtained nitrogen, potassium, phosphorus application rate from a global crop-specific fertilization dataset[53]. It should also be noted that current global data on irrigation and fertilizer inputs are generally derived from information aggregated at national or large-regional scales and do not capture fine-scale variations, though their nominal spatial resolution is high (for example, ref. 54), which also partially explain why the statistical model could not detect robustly their influence. This should not be interpreted as that irrigation and other management practices are not important.

Climatic and edaphic data

Climate variables used in this study, including daily maximum or minimum 2-m air temperature and precipitation, were obtained from China Meteorological Forcing Dataset[55] (CMFD, https://data.tpdc.ac.cn/zh-hans/data/e60dfd96-5fd8-493f-beae-e8e5d24dece4) for China, from the E-OBS[56] dataset (https://surfobs.climate.copernicus.eu/data-access/access_eobs.php) for Europe and from the PRISM[57] dataset (https://www.prism.oregonstate.edu/) for the USA, respectively. We also applied a bias-adjusted dataset using the WATCH Forcing Data methodology to surface meteorological variables from the ERA-5 reanalysis data (WFDE5, https://www.isimip.org/gettingstarted/input-data-bias-adjustment/details/114/)[58,59] to check the robustness to the input climate datasets (Supplementary Fig. 8). Downward surface solar radiation (R_s) and vapour pressure deficit were obtained from ERA-5 reanalysis datasets (https://cds.climate.copernicus.eu/). We obtained GLEAM4[60] root-zone soil moisture (https://www.gleam.eu/). Top soil (0–30 cm) characteristic data were retrieved from the Regridded Harmonized World Soil Database v.1.2 in the Oak Ridge

National Laboratory Distributed Active Archive Center for Biogeochemical Dynamics (https://www.fao.org/soils-portal/soil-survey/soil-maps-and-databases/harmonized-world-soil-database-v12/en/). Variables were resampled using average value in each administrative unit. The intra-county heterogeneities are not considered in this study (Supplementary Fig. 22).

Model simulation data

We used Phase 3 simulation results by Global Gridded Crop Model Inter-comparison of the Agricultural Model Inter-comparison and Improvement Project (AgMIP), including 11 process-based crop models: CROVER, CYGMA, DSSAT-Pythia, EPIC-IIASA, ISAM, LDNDC, LPJmL, pDSSAT, PEPIC, PROMET and SIMPLACE-LINTUL5+. Note that not all model simulated both crops, DSSAT-Pythia did not simulate soybean. These models are considered independent with different structures and assumptions; further details are described in Supplementary Table 2 and ref. 48. All crop models were driven by the same bias-adjusted weather dataset from five global climate models (GCM) in phase 6 of the coupled model intercomparison project (CMIP6)[48,61] at 0.5° × 0.5° spatial resolution, that is, GFDL-ESM4, IPSL-CM6A-LR, MPI-ESM1-2-HR, MRI-ESM2-0 and UKESM1-0-LL. These GCMs data were used to project future exposure in this study.

GGCM outputs including historical yield simulations and projected stages of growing period under SSP126 and SSP585 scenarios were used in this study. For some models who did not simulate anthesis, empirical flowering dates were set based on the averaged proportion of observational phenology period length in corresponding geographical units. Model outputs in the middle of the twenty-first century (2041–2060) and by the end of the twenty-first century (2081–2100) were included for future projections. All simulation data were resampled to subnational administrative units using regional averaged value, in accordance with the observational yield records.

Detection of $EDD_{threshold}$

Following the conventional concept which assume crop yield has a nonlinear thermal response[2,3], we calculated growing degree days (GDDs) and extreme degree days (EDDs):

$$GDD_{base,upper} = \frac{1}{24} \times \sum_{t=1}^{N} DD_t, DD = \begin{cases} T_{upper} - T_{base} & T_t \geq T_{upper} \\ T_t - T_{base} & T_{upper} > T_t \geq T_{base} \\ 0 & T_t < T_{base} \end{cases} \quad (1)$$

$$EDD = \frac{1}{24} \times \sum_{t=1}^{N} DD_t, DD = \begin{cases} T_t - EDD_{threshold} & T_t \geq EDD_{threshold} \\ 0 & T_t < EDD_{threshold} \end{cases} \quad (2)$$

where T_t is the hourly temperature calculated by sinusoidal interpolation between daily T_{min} and T_{max} following previous researches[3,17]. Degree days calculated by hourly temperature are regarded as a more accurate predictor of yield than daily temperature indicators[25]. N is the length of hours of county-specific growing period. EDD is a measure of exposure to temperatures above the extreme high-temperature threshold ($EDD_{threshold}$). Here we make $EDD_{threshold}$ equals to the T_{upper} of GDD. We also tested a piecewise GDD which divide $GDD_{base,upper}$ into $GDD_{base,opt}$ and $GDD_{opt,upper}$ using a crop-specific optimal temperature parameter, T_{opt}. The calculations of these GDD terms follow the description in equation (1).

The $EDD_{threshold}$ is defined as the air temperature at which EDD and GDD are best separated. Note that the threshold here is a statistical parameter in a dose–response function, not necessarily the same to the physiological constant under controlled experiment, and it reflects the onset of steep yield loss under local conditions. Canopy temperature is also of interest, but it is difficult to measure at large spatial and temporal scale because of the complexity of canopy structure and its interactions with microclimate[40,62]. Instead, the threshold of air temperature could be clearly defined and it provides a viable approach to investigate the variations. Further improvements to the extreme heat exposure estimation needs better accounting for the canopy temperature, which is part of the process that shaping the variation of the thresholds.

A multilinear regression was applied to each of the county to estimate the $EDD_{threshold}$. When estimating parameters for each county c, we only had a few observations at each county (up to 20 years); thus a time-series regression would not be able to reliably estimate the region-specific $EDD_{threshold}$. To overcome this limitation, we integrated spatial distance into our statistical model, which allow us to borrow data from nearby locations. For each county, we estimated the geodesic distance between the centroids of a county c_0 and its nearby counties and got a rank of proximity, denoted as

$$c_0, c_1, c_2, \ldots, c_i, \ldots, c_n \quad i = 0, 1, \ldots, n \quad (3)$$

where c_1 is the nearest county to c_0, c_2 is the second nearest county to c_0, c_i is the ist nearest county to c_0 and c_n is the farthest county to c_0. The total number of counties is n. In this point of view, our spatially generalized statistical model, as an extension of the linear regression framework, could be exemplified by the following equation

$$Y_{c_i,t} = \sum_{k=1}^{m} \beta_{k,c_i} X_{c_i,t} + C_{c_i} + \varepsilon_{c_i,t}, i = 0, 1, \ldots, r(0 \leq r \leq n) \quad (4)$$

where Y is the county-level yield, X contains m variables in county c_i and year t, C is a county-fixed constant which capture time-invariant effect and ε is an error term. We reported the results of X = (GDD, EDD, quadratic growing-season precipitation, quadratic yield trend). We also tested different specifications for the X in equation (4). (1) For GDD, a piecewise estimation of $GDD_{base,opt}$ and $GDD_{opt,upper}$ was applied (Supplementary Fig. 26a), instead of conventional $GDD_{base,upper}$. T_{min} and T_{opt} were defined according to Supplementary Table 3. (2) For the water-availability term, three proxies were tested, including precipitation for the 21-day period centred at anthesis (a period commonly recognized crops are more susceptible[3,33,41,63]), precipitation for the entire growing season and average root-zone soil moisture for the entire growing season. We also tested the alternative model using a linear precipitation term. (3) For the long-term trend of yield, linear or quadratic detrending was tested if the county had a significant trend; otherwise we subtracted the mean value. All these tests made little difference and gave similar distributions (Supplementary Figs. 3–7). Also, the distribution of $EDD_{threshold}$ estimations was robust to the different selections of the GDD parameters (Supplementary Figs. 1 and 2), and different choices of variables of X (Supplementary Figs. 9–11).

For each specific county, we implemented a data-borrowing scheme that includes the r nearest neighbouring counties into the regression. We tested different values of the spatial pooling radii (the parameter r) and found the distribution of $EDD_{threshold}$ remains similar when $r < 10$. The choice $r = 7$ corresponds to an effective neighbourhood scale of roughly 50 km on average, which is comparable to the 0.5° grid resolution of widely used global crop model simulations and gridded climate datasets. We also quantified uncertainty using a spatial block bootstrap and reported the standard deviation of the estimation. The uncertainty of the estimation of the threshold of extreme heat-induced yield loss in the majority counties is less than 2.5 °C (Supplementary Fig. 27).

We estimated equation (4) over all possible thresholds between T_{opt} (Supplementary Table 3) and the maximum air temperature within the entire growing season ($T^{air}_{max\,gs}$) by changing $EDD_{threshold}$ with a 0.2 °C step. For each possible $EDD_{threshold}$ value, corresponding GDD, EDD and root-mean-square error (RMSE) of the regression model were

calculated. Therefore, a temperature response curve of RMSE of the model was generated for each geographical unit. $EDD_{threshold}$ was selected as the best fit where RMSE was minimized (Supplementary Fig. 26b). Using other model fitness indicators, such as Akaike Information Criterion or Bayesian Information Criterion, gave very similar estimates (Supplementary Fig. 21).

We compared our new estimates on $EDD_{threshold}$ with heat thresholds reported by prior experimental studies (Supplementary Table 1). Our county-level estimates were generally consistent with thresholds observed from rain-fed field experiments but tended to be slightly lower than thresholds estimated under highly controlled chamber conditions. Compared with field experiments, controlled-environment experiment such as pot experiments can get different heat-threshold estimates because of factors including the artificially stable microclimate (constant day–night temperature regimes), the location of temperature measurement (for example, ambient air, canopy surface or within-canopy conditions) and the phenological stage at which plants were exposed to heat stress (for example, pre-flowering or heading). These experimental thresholds typically reflect physiologically grounded limits under controlled conditions, whereas our statistically derived thresholds can represent realized responses that integrate local environmental and management influences. We also applied an up-to-date machine learning method, extreme gradient boosting (XGBoost), to quantify and interpret the contributions and potential nonlinearity among climatic factors, soil factors and agronomic factors on $EDD_{threshold}$. Supplementary Notes provide more details.

We also tried to extend the length of time periods in the USA, where long-term county-level yield census are available, to 1981–2020 (Supplementary Fig. 28). We found that the patterns of $EDD_{threshold}$ remain stable in most counties, whereas higher values of thresholds have been shown in the latter period in around one-fifth counties for both maize and soybean. These changes could relate to the adoption to more extreme-resistant varieties[64,65] in the USA. Therefore, our results should be regarded as reflecting the distribution of $EDD_{threshold}$ over the first two decades of the twenty-first century.

We note that the value of $EDD_{threshold}$ in some mountainous or high-latitude regions (for example, Siberia and northeast China) should be treated with cautions because the extreme heat exposure of both crops remain rather limited (Supplementary Fig. 25). The scarce exposure implies $EDD_{threshold}$ may exceed contemporary range of temperature variations so that the statistical method is not applicable. Thus, only areas with more than 5 years of over 30 °C temperature exposure were preserved.

It should be noted that although we found relatively similar thresholds for the entire growing season as in the analysis with separate treatment of the anthesis and grain filling (AGF) stages (Supplementary Fig. 12), experimental evidence indicates that these thresholds could be dependent on the development stage. For instance, a previous review reported the maximum cardinal temperature of maize at anthesis is 37.3 °C, whereas the threshold is 36.0 °C during grain filling[66]. Understanding stage-specific thresholds might help farmers optimize both planting dates and cultivar selection custom-made to their specific regions. Future research could focus on this. In addition, there is a significant level of uncertainty involved in capturing phenology through remotely sensed products, as the interannual crop phenology variations are inevitable.

Following the same statistical equation, we applied the $EDD_{threshold}$ estimation on outputs of 11 crop models. We used simulated yield and corresponding climate variables from five GCMs, respectively. The results in Fig. 2a,b were the mean values across different climate and crop models (5 × 11 in total, DSSAT-Pythia did not simulate soybean).

Calculation of extreme heat exposure fraction

To evaluate the exposure to extreme heat of two crops, we estimated the exposure fraction difference as follows:

$$\mathrm{EF} = \frac{\sum_{t=1}^{N}\mu_t}{L} \times 100\%, \mu_t = \begin{cases} 1 & T_t \geq T_{\mathrm{base}} \\ 0 & T_t < T_{\mathrm{base}} \end{cases} \tag{5}$$

$$\text{exposure fraction difference} = \mathrm{EF}_{\mathrm{dynamic}} - \mathrm{EF}_{30^{\circ}\mathrm{C}} \tag{6}$$

where EF is the exposure fraction to extreme heat, T_t follows the definition in equation (2) and L is the length of growing season. $\mathrm{EF}_{\mathrm{dynamic}}$ denotes that T_{base} equals to our data-driven $EDD_{threshold}$ and $\mathrm{EF}_{30^{\circ}\mathrm{C}}$ denotes that T_{base} equals to 30 °C, the same as the threshold applied when the concept of EDD was first proposed[3]. Except to show the whole growing-season exposure fraction, we also illustrate the exposure fraction in the critical AGF stages. The extreme heat exposures for maize and soybean are more frequent during the AGF (Figs. 3 and 4). Moreover, we found that the surge in extreme heat exposure during anthesis cannot be compensated by the earlier flowering, which is induced by the acceleration of crop developments under warmer climates[34] (Supplementary Fig. 20).

Growing-season adaptation scenarios

The exposure to extreme heat could be altered through changing sowing date and the choice of cultivars. We estimated three potential adaptation managements by adjusting growing period: (1) apply time-constant growing-season length instead of heat-unit-dependent growing-season length used in crop models, assuming technological improvement through plant breeding by introducing long-maturity cultivars[32] to prolong growing season. (2) Apply adapted dynamic sowing dates instead of constant sowing dates used in crop models, assuming earlier planting under warming scenario to avoid terminal heat. (3) Apply (1) and (2) together. The growing season of crops are mostly temperature driven in the extratropical Northern Hemisphere[67]. Because the crop models use constant sowing dates for historical simulation and future scenarios, we applied dynamic sowing dates (D_{SOS}) in each scenario by calculating the cumulative temperature in degree days (DD):

$$\begin{cases} \sum_{d=1}^{D_{\mathrm{SOS}}-1} \mathrm{DD}_d < \mathrm{GDD0}_{\min} \\ \sum_{d=1}^{D_{\mathrm{SOS}}} \mathrm{DD}_d \geq \mathrm{GDD0}_{\min} \\ \mathrm{GDD0}_{\min} = \sum_{d=1}^{\overline{\mathrm{SOS}}} \mathrm{DD}_d, \mathrm{DD} = \begin{cases} T_d - T_{\min} & T_d \geq T_{\min} \\ 0 & T_d < T_{\min} \end{cases} \end{cases} \tag{7}$$

where D_{SOS} is the date of dynamic sowing dates under future scenario, d denotes the day of year and $\mathrm{GDD0}_{\min}$ is the minimum running accumulation of DD above $T_{\min}$ before sowing. $T_{\min}$ follows the definition in equation (1), and their values can be found in Supplementary Table 3. $\overline{\mathrm{SOS}}$ is the averaged sowing day of growing season in historical period. The average dynamic sowing dates in the study area are projected to advance for a few days under SSP126 and for nearly a month under SSP585 by 2100 due to earlier spring (Supplementary Fig. 29).

Reporting summary

Further information on research design is available in the Nature Portfolio Reporting Summary linked to this article.

Data availability

The air temperature threshold patterns for maize and soybean are available via Zenodo at https://doi.org/10.5281/zenodo.17142122 (ref. 68). Data supporting the findings of this study are available within the article and/or its Supplementary Information files. Cropland distributions are from USDA Cropland Data Layer (https://www.nass.usda.gov/Research_and_Science/Cropland/Release/index.php) and MapSPAM (https://mapspam.info/data/). Phenology data are from USDA National

Agricultural Statistics Service (www.nass.usda.gov), China Meteorological Administration (data.cma.cn) and ChinaCropPhen (https://doi.org/10.6084/m9.figshare.8313530), and European Phenology data can be accessed upon request to G.Z. at gang.zhao@nwafu.edu.cn. Yield data are from USDA National Agricultural Statistics Service (www.nass.usda.gov), Eurostat (https://ec.europa.eu/eurostat) and Russian Federal State Statistics Service (https://rosstat.gov.ru/). Global production data in Fig. 1 is based on data from Food and Agriculture Organization of the United Nations (FAO, www.fao.org/faostat). Climate data are from China Meteorological Forcing Dataset (CMFD, https://data.tpdc.ac.cn/zh-hans/data/e60dfd96-5fd8-493f-beae-e8e5d24dece4), E-OBS (https://surfobs.climate.copernicus.eu/dataaccess/access_eobs.php), PRISM (https://www.prism.oregonstate.edu/), WFDE5 (https://www.isimip.org/gettingstarted/input-data-bias-adjustment/details/114/) and ERA-5 reanalysis datasets (https://cds.climate.copernicus.eu/). Regridded Harmonized World Soil Database v.1.2 is available at https://www.fao.org/soils-portal/soil-survey/soil-maps-and-databases/harmonized-world-soil-database-v12/en/. The GGCMI crop calendar is accessible at https://doi.org/10.5281/zenodo.5062513. GGCMI phase 3 data can be accessed at https://data.isimip.org/search/tree/ISIMIP3b/OutputData/agriculture/. GLEAM4 dataset can be accessed at https://www.gleam.eu/. Global crop-specific fertilization dataset is available at https://doi.org/10.6084/m9.figshare.25435432. The country-level boundaries are obtained from publicly accessible websites. World map and counties boundaries in the USA are from https://www.naturalearthdata.com/downloads/10m-cultural-vectors/, in the European Union from https://ec.europa.eu/eurostat/web/gisco/geodata/statistical-units/territorial-units-statistics, in Russia from https://simplemaps.com/gis/country/ru and in China from https://cloudcenter.tianditu.gov.cn/administrativeDivision/. Source data are provided with this paper.

Code availability

The analyses were processed using MATLAB R2020a, ArcGIS 10.4 and Python 3.7. The code files can be accessed via figshare at https://figshare.com/s/ea100e809648d85f2c77 (ref. 69).

References

1. *AR6 Synthesis Report: Climate Change 2023* (IPCC, 2023).
2. Schlenker, W. & Roberts, M. J. Nonlinear temperature effects indicate severe damages to US crop yields under climate change. *Proc. Natl Acad. Sci. USA* **106**, 15594–15598 (2009).
3. Lobell, D. B., Baenziger, M., Magorokosho, C. & Vivek, B. Nonlinear heat effects on African maize as evidenced by historical yield trials. *Nat. Clim. Change* **1**, 42–45 (2011).
4. Schauberger, B. et al. Consistent negative response of US crops to high temperatures in observations and crop models. *Nat. Commun.* **8**, 13931 (2017).
5. Rezaei, E. E. et al. Climate change impacts on crop yields. *Nat. Rev. Earth Environ.* **4**, 831–846 (2023).
6. Lobell, D. B., Sibley, A. & Ivan Ortiz-Monasterio, J. Extreme heat effects on wheat senescence in India. *Nat. Clim. Change* **2**, 186–189 (2012).
7. Lesk, C., Rowhani, P. & Ramankutty, N. Influence of extreme weather disasters on global crop production. *Nature* **529**, 84–87 (2016).
8. Vogel, E. et al. The effects of climate extremes on global agricultural yields. *Environ. Res. Lett.* **14**, 054010 (2019).
9. Tigchelaar, M., Battisti, D. S., Naylor, R. L. & Ray, D. K. Future warming increases probability of globally synchronized maize production shocks. *Proc. Natl Acad. Sci. USA* **115**, 6644–6649 (2018).
10. Xie, W. et al. Decreases in global beer supply due to extreme drought and heat. *Nat. Plants* **4**, 964–973 (2018).
11. Wheeler, T. & von Braun, J. Climate change impacts on global food security. *Science* **341**, 508–513 (2013).
12. Gourdji, S. M., Sibley, A. M. & Lobell, D. B. Global crop exposure to critical high temperatures in the reproductive period: historical trends and future projections. *Environ. Res. Lett.* **8**, 024041 (2013).
13. Jackson, N. D., Konar, M., Debaere, P. & Sheffield, J. Crop-specific exposure to extreme temperature and moisture for the globe for the last half century. *Environ. Res. Lett.* **16**, 064006 (2021).
14. Sabir, K. et al. Stage-specific genotype-by-environment interactions determine yield components in wheat. *Nat. Plants* **9**, 1688–1696 (2023).
15. Qaseem, M. F., Qureshi, R. & Shaheen, H. Effects of pre-anthesis drought, heat and their combination on the growth, yield and physiology of diverse wheat (*Triticum aestivum* L.) genotypes varying in sensitivity to heat and drought stress. *Sci. Rep.* **9**, 6955 (2019).
16. Lesk, C. et al. Compound heat and moisture extreme impacts on global crop yields under climate change. *Nat. Rev. Earth Environ.* **3**, 872–889 (2022).
17. Lobell, D. B. et al. The critical role of extreme heat for maize production in the United States. *Nat. Clim. Change* **3**, 497–501 (2013).
18. BarnabÁs, B., JÄger, K. & FehÉr, A. The effect of drought and heat stress on reproductive processes in cereals. *Plant Cell Environ.* **31**, 11–38 (2008).
19. Carter, E. K., Melkonian, J., Riha, S. J. & Shaw, S. B. Separating heat stress from moisture stress: analyzing yield response to high temperature in irrigated maize. *Environ. Res. Lett.* **11**, 094012 (2016).
20. Siebert, S., Webber, H., Zhao, G. & Ewert, F. Heat stress is overestimated in climate impact studies for irrigated agriculture. *Environ. Res. Lett.* **12**, 054023 (2017).
21. Jian, H. et al. Supplemental irrigation mitigates yield loss of maize through reducing canopy temperature under heat stress. *Agric. Water Manage.* **299**, 108888 (2024).
22. Gabaldón-Leal, C. et al. Modelling the impact of heat stress on maize yield formation. *Field Crops Res.* **198**, 226–237 (2016).
23. Martinez-Villalobos, C., Fu, D., Loikith, P. C. & Neelin, J. D. Accelerating increase in the duration of heatwaves under global warming. *Nat. Geosci.* **18**, 716–723 (2025).
24. IPCC. *Climate Change 2021: The Physical Science Basis* (Cambridge Univ. Press, 2021).
25. Tack, J., Barkley, A. & Nalley, L. L. Effect of warming temperatures on US wheat yields. *Proc. Natl Acad. Sci. USA* **112**, 6931–6936 (2015).
26. Wang, N. et al. Modelling maize phenology, biomass growth and yield under contrasting temperature conditions. *Agric. For. Meteorol.* **250-251**, 319–329 (2018).
27. Butler, E. E. & Huybers, P. Variations in the sensitivity of US maize yield to extreme temperatures by region and growth phase. *Environ. Res. Lett.* **10**, 034009 (2015).
28. Huang, M. et al. Assessing maize potential to mitigate the adverse effects of future rising temperature and heat stress in China. *Agric. For. Meteorol.* **311**, 108673 (2021).
29. Zhu, P. et al. Warming reduces global agricultural production by decreasing cropping frequency and yields. *Nat. Clim. Change* **12**, 1016–1023 (2022).
30. Xiong, W. et al. New wheat breeding paradigms for a warming climate. *Nat. Clim. Change* **14**, 869–875 (2024).
31. Schewe, J. et al. State-of-the-art global models underestimate impacts from climate extremes. *Nat. Commun.* **10**, 1005 (2019).
32. Minoli, S., Jägermeyr, J., Asseng, S., Urfels, A. & Müller, C. Global crop yields can be lifted by timely adaptation of growing periods to climate change. *Nat. Commun.* **13**, 7079 (2022).
33. Teixeira, E. I., Fischer, G., van Velthuizen, H., Walter, C. & Ewert, F. Global hot-spots of heat stress on agricultural crops due to climate change. *Agric. For. Meteorol.* **170**, 206–215 (2013).

34. Rezaei, E. E., Siebert, S. & Ewert, F. Intensity of heat stress in winter wheat—phenology compensates for the adverse effect of global warming. *Environ. Res. Lett.* **10**, 024012 (2015).
35. Zandalinas, S. I., Mittler, R., Balfagón, D., Arbona, V. & Gómez-Cadenas, A. Plant adaptations to the combination of drought and high temperatures. *Physiol. Plant.* **162**, 2–12 (2018).
36. Kan, Y., Mu, X.-R., Gao, J., Lin, H.-X. & Lin, Y. The molecular basis of heat stress responses in plants. *Mol. Plant* **16**, 1612–1634 (2023).
37. Rosa, L. et al. Potential for sustainable irrigation expansion in a 3 °C warmer climate. *Proc. Natl Acad. Sci. USA* **117**, 29526–29534 (2020).
38. Webber, H. et al. Canopy temperature for simulation of heat stress in irrigated wheat in a semi-arid environment: a multi-model comparison. *Field Crops Res.* **202**, 21–35 (2017).
39. Siebert, S., Ewert, F., Eyshi Rezaei, E., Kage, H. & Graß, R. Impact of heat stress on crop yield—on the importance of considering canopy temperature. *Environ. Res. Lett.* **9**, 044012 (2014).
40. Still, C. J. et al. Imaging canopy temperature: shedding (thermal) light on ecosystem processes. *New Phytol.* **230**, 1746–1753 (2021).
41. Eyshi Rezaei, E., Webber, H., Gaiser, T., Naab, J. & Ewert, F. Heat stress in cereals: mechanisms and modelling. *Eur. J. Agron.* **64**, 98–113 (2015).
42. Müller, C. et al. Substantial differences in crop yield sensitivities between models call for functionality-based model evaluation. *Earth's Future* **12**, e2023EF003773 (2024).
43. Zabel, F. et al. Large potential for crop production adaptation depends on available future varieties. *Glob. Change Biol.* **27**, 3870–3882 (2021).
44. Parent, B. et al. Maize yields over Europe may increase in spite of climate change, with an appropriate use of the genetic variability of flowering time. *Proc. Natl Acad. Sci. USA* **115**, 10642–10647 (2018).
45. Lipper, L. et al. Climate-smart agriculture for food security. *Nat. Clim. Change* **4**, 1068–1072 (2014).
46. Schauberger, B., Kato, H., Kato, T., Watanabe, D. & Ciais, P. French crop yield, area and production data for ten staple crops from 1900 to 2018 at county resolution. *Sci. Data* **9**, 38 (2022).
47. Luo, Y., Zhang, Z., Chen, Y., Li, Z. & Tao, F. ChinaCropPhen1km: a high-resolution crop phenological dataset for three staple crops in China during 2000–2015 based on leaf area index (LAI) products. *Earth Syst. Sci. Data* **12**, 197–214 (2020).
48. Jagermeyr, J. et al. Climate impacts on global agriculture emerge earlier in new generation of climate and crop models. *Nat. Food* **2**, 873–885 (2021).
49. *Global Spatially-Disaggregated Crop Production Statistics Data for 2010 Version 2.0* (International Food Policy Research Institute, 2019).
50. Xie, Y., Gibbs, H. K. & Lark, T. J. Landsat-based Irrigation Dataset (LANID): 30-m resolution maps of irrigation distribution, frequency, and change for the U.S., 1997–2017. *Earth Syst. Sci. Data* **13**, 5689–5710 (2021).
51. Zhang, C., Dong, J. & Ge, Q. Mapping 20 years of irrigated croplands in China using MODIS and statistics and existing irrigation products. *Sci. Data* **9**, 407 (2022).
52. Boryan, C., Yang, Z. W., Mueller, R. & Craig, M. Monitoring US agriculture: the US Department of Agriculture, National Agricultural Statistics Service, Cropland Data Layer Program. *Geocarto Int.* **26**, 341–358 (2011).
53. Coello, F. et al. Global crop-specific fertilization dataset from 1961–2019. *Sci. Data* **12**, 40 (2025).
54. Siebert, S. et al. Development and validation of the global map of irrigation areas. *Hydrol. Earth Syst. Sci.* **9**, 535–547 (2005).
55. Kun, Y. & Jie, H. *China Meteorological Forcing Dataset (1979–2018)* (Center National Tibetan Plateau Data, 2019).
56. Cornes, R. C., van der Schrier, G., van den Besselaar, E. J. M. & Jones, P. D. An ensemble version of the E-OBS temperature and precipitation data sets. *J. Geophys. Res. Atmos.* **123**, 9391–9409 (2018).
57. Daly, C. et al. Physiographically sensitive mapping of climatological temperature and precipitation across the conterminous United States. *Int. J. Climatol.* **28**, 2031–2064 (2008).
58. Cucchi, M. et al. WFDE5: bias-adjusted ERA5 reanalysis data for impact studies. *Earth Syst. Sci. Data* **12**, 2097–2120 (2020).
59. Lange, S. et al. WFDE5 over land merged with ERA5 over the ocean (W5E5 v2.0) (ISIMIP Repository, 2021).
60. Miralles, D. G. et al. GLEAM4: global land evaporation dataset at 0.1° resolution from 1980 to near present. *Sci. Data* **12**, 416 (2025).
61. Lange, S. Trend-preserving bias adjustment and statistical downscaling with ISIMIP3BASD (v1.0). *Geosci. Model Dev.* **12**, 3055–3070 (2019).
62. Garen, J. C. et al. Canopy-top measurements do not accurately quantify canopy-scale leaf thermoregulation. *Proc. Natl Acad. Sci. USA* **120**, e2301914120 (2023).
63. Prasad, P. V. V., Bheemanahalli, R. & Jagadish, S. V. K. Field crops and the fear of heat stress—opportunities, challenges and future directions. *Field Crops Res.* **200**, 114–121 (2017).
64. Gaffney, J. et al. Industry-scale evaluation of maize hybrids selected for increased yield in drought-stress conditions of the US corn belt. *Crop Sci.* **55**, 1608–1618 (2015).
65. Cooper, M. & Messina, C. D. Breeding crops for drought-affected environments and improved climate resilience. *Plant Cell* **35**, 162–186 (2023).
66. Sanchez, B., Rasmussen, A. & Porter, J. R. Temperatures and the growth and development of maize and rice: a review. *Glob. Change Biol.* **20**, 408–417 (2014).
67. Waha, K., van Bussel, L. G. J., Müller, C. & Bondeau, A. Climate-driven simulation of global crop sowing dates. *Glob. Ecol. Biogeogr.* **21**, 247–259 (2012).
68. Zhao, Q. Dataset for "Temperature thresholds of extreme heat-induced yield loss in maize and soybean reveal geographic heterogeneity across the Northern Hemisphere". *Zenodo* https://doi.org/10.5281/zenodo.17142122 (2025).
69. Zhao, Q. et al. Code for paper "Temperature thresholds of extreme heat-induced yield loss in maize and soybean reveal geographic heterogeneity across the Northern Hemisphere". *figshare* https://figshare.com/s/ea100e809648d85f2c77 (2026).

Acknowledgements

This study was supported by the Scientific Research Innovation Capability Support Project for Young Faculty (ZYGXQNJSKYCXNLZCXM-S2), the National Key R&D Program of China (2024YFF0809103) and the National Natural Science Foundation of China (42171096). C.W. was supported by Horizon Europe research and innovation programme under the Marie Skłodowska-Curie grant agreement no. 101154967 and the Leibniz Female Professorship Award (application no. P102/2020). We thank A. Senthold for his helpful comment on an earlier version of this paper.

Author contributions

X.W. designed the study. Q.Z. collected statistical data and plotted all figures. Q.Z. and C.W. performed the analyses. G.Z. provided European phenology data. C.W., C.M., H.W., C.F., A.J., W.L., M.O., F. Zabel, J.J. and Y.J. provided crop model simulation data and experiment data. Q.Z., C.W. and X.W. wrote the first draft of the paper. All authors contributed to interpretation of the results and revision of the paper.

Competing interests

The authors declare no competing interests.

Additional information

Extended data is available for this paper at https://doi.org/10.1038/s43016-026-01298-0.

Supplementary information The online version contains supplementary material available at https://doi.org/10.1038/s43016-026-01298-0.

Correspondence and requests for materials should be addressed to Xuhui Wang.

Peer review information *Nature Food* thanks Chongyang Xu, Tao Ye and the other, anonymous, reviewer(s) for their contribution to the peer review of this work.

Reprints and permissions information is available at www.nature.com/reprints.

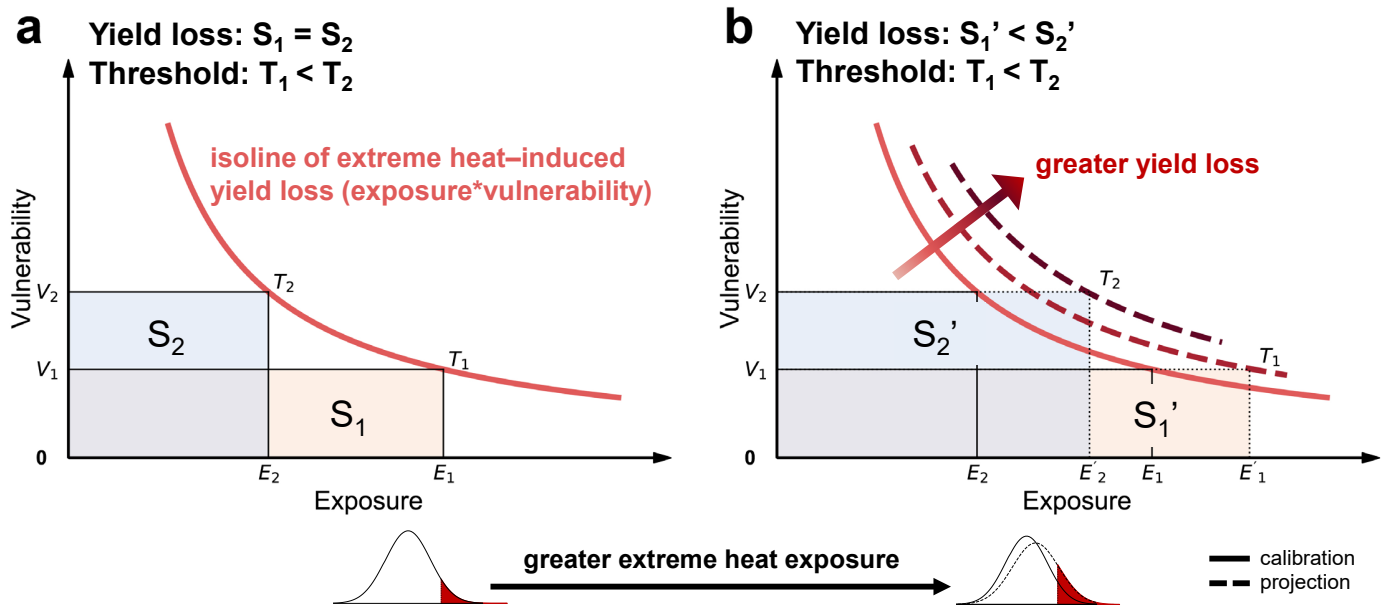
Publisher's note Springer Nature remains neutral with regard to jurisdictional claims in published maps and institutional affiliations.

Springer Nature or its licensor (e.g. a society or other partner) holds exclusive rights to this article under a publishing agreement with the author(s) or other rightsholder(s); author self-archiving of the accepted manuscript version of this article is solely governed by the terms of such publishing agreement and applicable law.

© The Author(s), under exclusive licence to Springer Nature Limited 2026

[1]Institute of Carbon Neutrality, Sino-French Institute for Earth System Sciences, College of Urban and Environmental Sciences, Peking University, Beijing, China. [2]Leibniz Centre for Agricultural Landscape Research (ZALF), Müncheberg, Germany. [3]Potsdam Institute for Climate Impact Research (PIK), Member of the Leibniz Association, Potsdam, Germany. [4]CSIRO Agriculture and Food, Canberra, Australian Capital Territory, Australia. [5]Institute of Environmental Sciences, Brandenburg University of Technology, Cottbus, Germany. [6]State Key Laboratory of Soil and Water Conservation and Desertification Control, College of Soil and Water Conservation Science and Engineering, Northwest A&F University, Yangling, China. [7]BASF Digital Farming GmbH, Cologne, Germany. [8]Biodiversity and Natural Resources Program, International Institute for Applied Systems Analysis, Laxenburg, Austria. [9]Department of Climate, Meteorology and Atmospheric Sciences, University of Illinois, Urbana-Champaign, IL, USA. [10]State Key Laboratory of Efficient Utilization of Agricultural Water Resources, China Agricultural University, Beijing, China. [11]Center for Climate Change Adaptation, National Institute for Environmental Studies, Tsukuba, Japan. [12]Department of Environmental Sciences, University of Basel, Basel, Switzerland. [13]Climate School, Columbia University, New York, NY, USA. [14]NASA Goddard Institute for Space Studies, New York, NY, USA. [15]Jiangsu Collaborative Innovation Center for Modern Crop Production/Key Laboratory of Crop Physiology and Ecology in Southern China, College of Agriculture, Nanjing Agricultural University, Nanjing, China. [16]These authors contributed equally: Quanbo Zhao, Chenzhi Wang. ✉e-mail: xuhui.wang@pku.edu.cn

https://doi.org/10.1038/s43016-026-01298-0



Extended Data Fig. 1 | Conceptual diagram of how model underestimate in EDD threshold leads to its underestimate in extreme heat-induced yield loss. The extreme heat-induced yield loss (the color-shaded area) could be understood as the product of exposure (cumulated by EDD, x-axis) and vulnerability (marginal damage per unit extreme heat exposure, y-axis). **a**. Models can estimate similar extreme heat-induced yield loss (yield loss isoline, $S_1 = S_2$) with the trade-off in estimating the exposure and the vulnerability (that is lower EDD threshold ($T_1 < T_2$) leads to higher estimates on exposure ($E_1 > E_2$), which has to be balanced with lower estimates on vulnerability ($V_1 < V_2$)). **b**. When warming induces greater extreme heat exposure, models with underestimated EDD threshold ($T_1 < T_2$) and thus underestimated vulnerability ($V_1 < V_2$) will project underestimated yield loss ($S_1' < S_2'$).

nature portfolio

Corresponding author(s): Xuhui, Wang

Last updated by author(s): Dec 3, 2025

Reporting Summary

Nature Portfolio wishes to improve the reproducibility of the work that we publish. This form provides structure for consistency and transparency in reporting. For further information on Nature Portfolio policies, see our Editorial Policies and the Editorial Policy Checklist.

Statistics

For all statistical analyses, confirm that the following items are present in the figure legend, table legend, main text, or Methods section.

n/a	Confirmed
☐	☒ The exact sample size (*n*) for each experimental group/condition, given as a discrete number and unit of measurement
☒	☐ A statement on whether measurements were taken from distinct samples or whether the same sample was measured repeatedly
☐	☒ The statistical test(s) used AND whether they are one- or two-sided *Only common tests should be described solely by name; describe more complex techniques in the Methods section.*
☒	☐ A description of all covariates tested
☐	☒ A description of any assumptions or corrections, such as tests of normality and adjustment for multiple comparisons
☐	☒ A full description of the statistical parameters including central tendency (e.g. means) or other basic estimates (e.g. regression coefficient) AND variation (e.g. standard deviation) or associated estimates of uncertainty (e.g. confidence intervals)
☐	☒ For null hypothesis testing, the test statistic (e.g. *F*, *t*, *r*) with confidence intervals, effect sizes, degrees of freedom and *P* value noted *Give P values as exact values whenever suitable.*
☒	☐ For Bayesian analysis, information on the choice of priors and Markov chain Monte Carlo settings
☒	☐ For hierarchical and complex designs, identification of the appropriate level for tests and full reporting of outcomes
☒	☐ Estimates of effect sizes (e.g. Cohen's *d*, Pearson's *r*), indicating how they were calculated

Our web collection on statistics for biologists contains articles on many of the points above.

Software and code

Policy information about availability of computer code

Data collection	No software was used to collect data. The source of datasets are listed below and in the article.
Data analysis	The analyses were performed using MATLAB R2020a, Python 3.7 and ArcGIS 10.4. Details were reported in the article.

For manuscripts utilizing custom algorithms or software that are central to the research but not yet described in published literature, software must be made available to editors and reviewers. We strongly encourage code deposition in a community repository (e.g. GitHub). See the Nature Portfolio guidelines for submitting code & software for further information.

Data

Policy information about availability of data

All manuscripts must include a data availability statement. This statement should provide the following information, where applicable:

- Accession codes, unique identifiers, or web links for publicly available datasets
- A description of any restrictions on data availability
- For clinical datasets or third party data, please ensure that the statement adheres to our policy

Data supporting the findings of this study are available within the article and/or its supplementary information files. Yield data: USDA National Agricultural Statistics Serves (www.nass.usda.gov), Eurostat (https://ec.europa.eu/eurostat), Russian Federal State Statistics Service (https://rosstat.gov.ru/). Global production data in Fig.1 based on data from Food and Agriculture Organization of the United Nations (FAO, www.fao.org/faostat). Cropland distributions: USDA Cropland Data Layer (https://www.nass.usda.gov/Research_and_Science/Cropland/Release/index.php), MapSPAM (https://mapspam.info/data/). Phenology data: USDA National

Agricultural Statistics Serves (www.nass.usda.gov), China Meteorological Administration (data.cma.cn), ChinaCropPhen (https://figshare.com/articles/dataset/ChinaCropPhen1km_A_high-resolution_crop_phenological_dataset_for_three_staple_crops_in_China_during_2000-2015_based_on_LAI_products/8313530), European Phenology data can be accessed upon request to Dr. Gang Zhao (gang.zhao@nwafu.edu.cn). Climate data: China Meteorological Forcing Dataset (CMFD, http://poles.tpdc.ac.cn/en/data/8028b944-daaa-4511-8769-965612652c49/), E-OBS (https://surfobs.climate.copernicus.eu/dataaccess/access_eobs.php), PRISM (https://www.prism.oregonstate.edu/), WFDE5 (https://www.isimip.org/gettingstarted/input-data-bias-adjustment/details/114/), ERA-5 reanalysis datasets (https://cds.climate.copernicus.eu/). Regridded Harmonized World Soil Database v.1.2 (https://www.fao.org/soils-portal/soil-survey/soil-maps-and-databases/harmonized-world-soil-database-v12/en/). The GGCMI crop calendar is accessible at https://doi.org/10.5281/zenodo.5062513. GGCMI phase3 data can be accessed at https://data.isimip.org/search/tree/ISIMIP3b/OutputData/agriculture/.

Human research participants

Policy information about studies involving human research participants and Sex and Gender in Research.

Reporting on sex and gender	*Use the terms sex (biological attribute) and gender (shaped by social and cultural circumstances) carefully in order to avoid confusing both terms. Indicate if findings apply to only one sex or gender; describe whether sex and gender were considered in study design whether sex and/or gender was determined based on self-reporting or assigned and methods used. Provide in the source data disaggregated sex and gender data where this information has been collected, and consent has been obtained for sharing of individual-level data; provide overall numbers in this Reporting Summary. Please state if this information has not been collected. Report sex- and gender-based analyses where performed, justify reasons for lack of sex- and gender-based analysis.*
Population characteristics	*Describe the covariate-relevant population characteristics of the human research participants (e.g. age, genotypic information, past and current diagnosis and treatment categories). If you filled out the behavioural & social sciences study design questions and have nothing to add here, write "See above."*
Recruitment	*Describe how participants were recruited. Outline any potential self-selection bias or other biases that may be present and how these are likely to impact results.*
Ethics oversight	*Identify the organization(s) that approved the study protocol.*

Note that full information on the approval of the study protocol must also be provided in the manuscript.

Field-specific reporting

Please select the one below that is the best fit for your research. If you are not sure, read the appropriate sections before making your selection.

☐ Life sciences ☐ Behavioural & social sciences ☒ Ecological, evolutionary & environmental sciences

For a reference copy of the document with all sections, see nature.com/documents/nr-reporting-summary-flat.pdf

Ecological, evolutionary & environmental sciences study design

All studies must disclose on these points even when the disclosure is negative.

Study description	We assessed the spatial variability of the critical temperature threshold of crop heat exposure based on 2001-2020 county-level statistical yield census (3929 counties for maize and 3779 counties for soybean) and simulations by eleven global gridded crop models, and projected the heat exposure till the end of the 21st century under two SSP scenarios, SSP126 and SSP585.
Research sample	The data we used were obtained from published sources, details can be seen in the Methods section.
Sampling strategy	N/A
Data collection	We collected the crop yield data based on regional statistical records from the government websites. Other data and their sources were given in the Data Availability part.
Timing and spatial scale	N/A
Data exclusions	The yield data were subjected to an outlier filtering, since the statistical annotations were sometimes erroneous with unattainable value. We included only regions with more than ten consecutive years. To identify the heat exposure threshold, we filtered regions where cropland had more than at least five years heat exposure (technically, daily maximum temperature>30℃ for more than one day within growing season) to assure the regions involved in the analysis did have experienced high temperature.
Reproducibility	N/A
Randomization	N/A
Blinding	N/A

Did the study involve field work? ☐ Yes ☒ No

Reporting for specific materials, systems and methods

We require information from authors about some types of materials, experimental systems and methods used in many studies. Here, indicate whether each material, system or method listed is relevant to your study. If you are not sure if a list item applies to your research, read the appropriate section before selecting a response.

Materials & experimental systems

n/a	Involved in the study
☒	☐ Antibodies
☒	☐ Eukaryotic cell lines
☒	☐ Palaeontology and archaeology
☒	☐ Animals and other organisms
☒	☐ Clinical data
☒	☐ Dual use research of concern

Methods

n/a	Involved in the study
☒	☐ ChIP-seq
☒	☐ Flow cytometry
☒	☐ MRI-based neuroimaging